Supporting Information

Scalable Assembly of Micron Boron Nitride into High-Temperature-Resistant Insulating Papers with Superior Thermal Conductivity

Meng-Xin Liu,[a] Rui-Yu Ma,[a] Zhi-Xing Wang,[b] Zhuo-Yang Li,[c] Gui-Lin Song,[a] Jie Lin,[a] Xin-Yuan Li,[a] Ling Xu,*[c] Ding-Xiang Yan,[c] Li-Chuan Jia,*[b] and Zhong-Ming Li[a]

[a] College of Polymer Science and Engineering, State Key Laboratory of Polymer Materials Engineering, Sichuan University, Chengdu, 610065, China

[b] College of Electrical Engineering, Sichuan University, Chengdu, 610065, China

[c] School of Aeronautics and Astronautics, Sichuan University, Chengdu, 610065, China

E-mail: lingxu@scu.edu.cn

E-mail: lcjia@scu.edu.cn

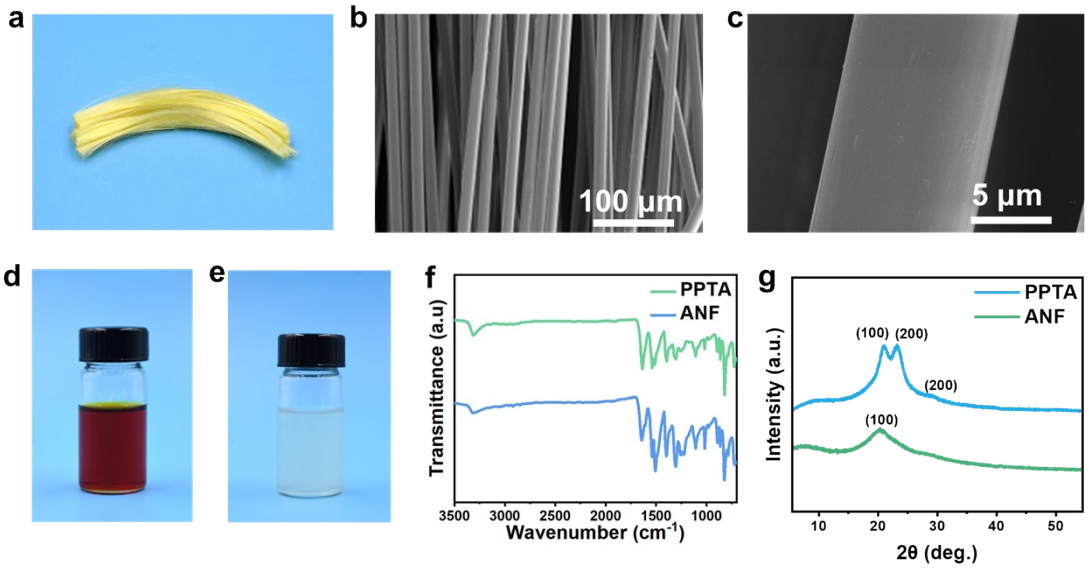

Fig. S1 (a) Digital photograph of PPTA fibers. (b) SEM image and (c) magnified SEM image of PPTA fibers. (d) Digital photograph of ANF/DMSO dispersion. (e) Digital photograph of ANF dispersion. (f) FTIR spectra of PPTA fibers and ANF. (g) XRD pattern of PPTA fibers and ANF.

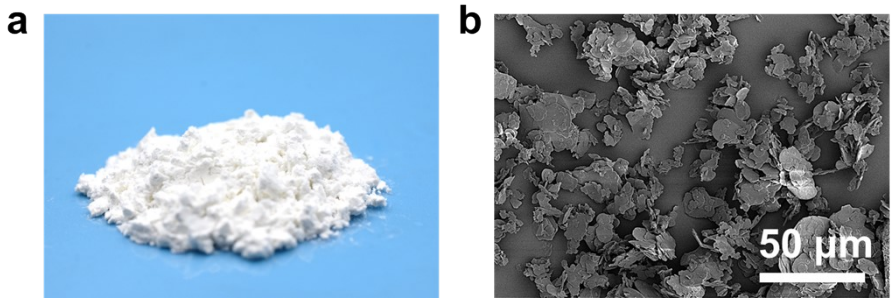

Fig. S2 (a) Digital photograph of m-BN powder. (b) SEM image of m-BN powder.

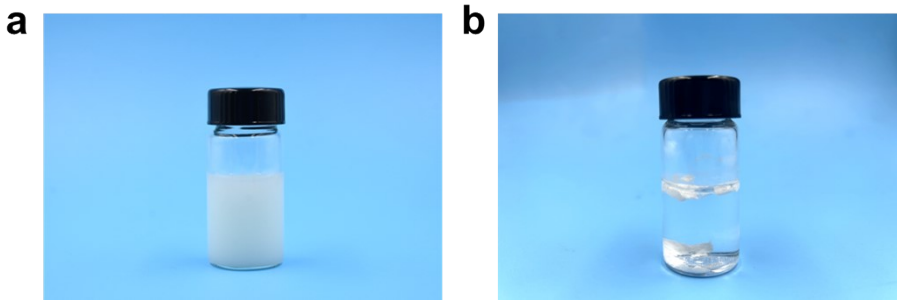

Fig. S3 Digital photograph of (a) m-BN@ANF ink and (b) m-BN dispersion after static storage for 30 days.

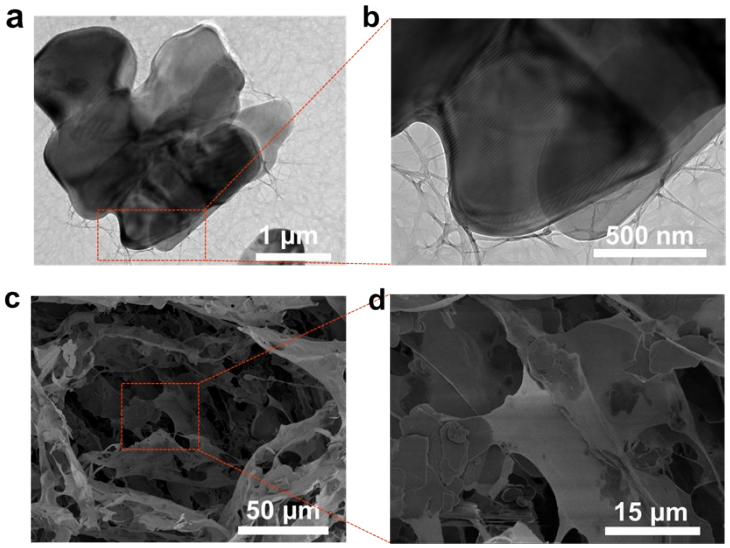

Fig. S4 (a) TEM and (b) magnified TEM images of m-BN@ANF ink. (c) SEM and (d) magnified SEM images of m-BN@ANF slurry.

Fig. S5 (a) Digital photograph of large quantities of m-BN@ANF ink after static storage for 30 days.

Density functional theory (DFT) calculations

The m-BN@ANF was studied by density functional theory (DFT). All calculations were performed via Vienna *ab initio* simulation package 6.1.0 (VASP) with the projector augmented wave (PAW) pseudopotentials.[1,2] The exchange-correlation interaction was calculated by the generalized gradient approximation (GGA) method with the spin-polarized Perdew−Burke−Ernzerhof (PBE) pure functional.[3] The long-

range van der Waals (vdW) interactions were handled by Grimme's DFT-D3 scheme.[4] The vacuum layer was set to 15 Å avoiding the interaction among mirror images.[5] For the parameters of calculations, the kinetic energy cutoff for the plane-wave basis set was chosen as 500 eV. Electronic energy was considered self-consistent when the energy change was smaller than 10^{-5} eV. Gaussian smearing with a width of σ=0.1 eV was set for the occupation of the electronic levels.[6] As for the structure optimization, all atoms were allowed to fully relax with the conjugate gradient method until the maximum force on any atom was smaller than 0.02 eV/Å. The Brillouin zone was sampled with 2×2×2 Monkhorst-Pack k-points grids.

Adsorption energy describes the decrease in energy when two materials combine during adsorption, it can be used to characterize the difficulty level of synthesizing compounds from components. The adsorption energy (E_{ads}) is defined as $E_{ads} = E_{total} - E_{adsorbate} - E_{substrate}$, where E_{total}, $E_{adsorbate}$ and $E_{substrate}$ are the total energy of the optimized adsorbate/substrate system, and the energy of the adsorbent structure and substrate structure, respectively. When the adsorption energy is negative, it represents the presence of interactions between the components, and if it is positive, it is not easy to form interaction.

In this system, based on the computational m-BN@ANF mixture model, the adsorption energy of mixture is calculated as follows: $E_{ads} = E_{m-BN@ANF} - E_{m-BN} - E_{ANF}$, where $E_{m-BN@ANF}$ represents the total energy of the m-BN@ANF mixture after adsorption, while E_{m-BN} and E_{ANF} represent the total energies of the isolated m-BN and ANF molecules, respectively.

Table S1. The adsorption energies between m-BN platelets and ANF.

E_{m-BN}	E_{ANF}	$E_{m-BN@ANF}$	E_{ads}
-865.817 eV	-200.617 eV	-1067.605 eV	-1.171 eV

The adsorption energy of the m-BN@ANF mixture was calculated as -1.171 eV, indicating the presence of non-negligible interactions between m-BN and ANF.

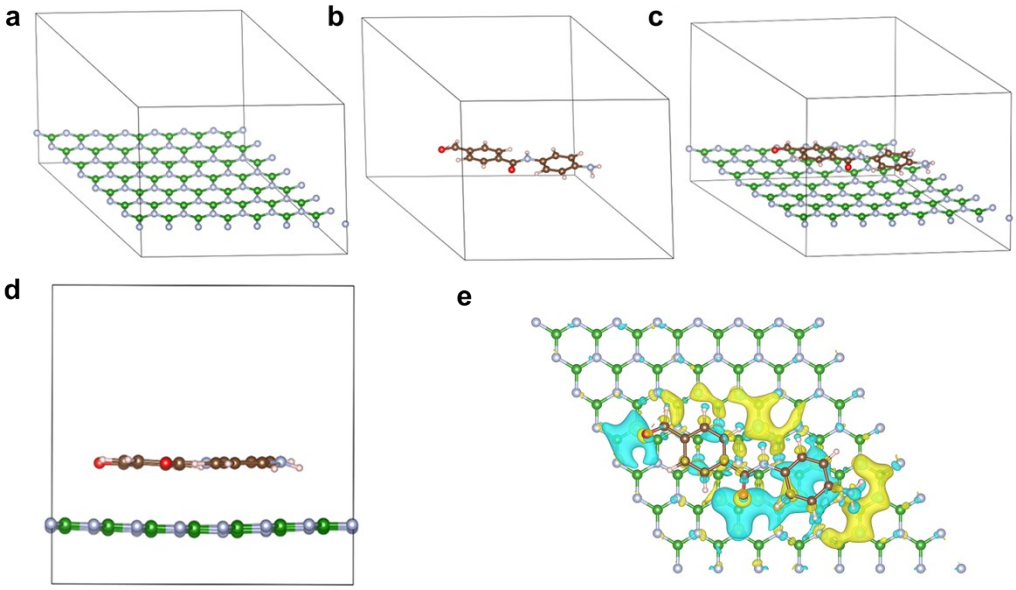

Fig. S6 (a-d) The optimized geometries for studied species, where white, green, brown, blue, and red balls are H, B, C, N, and O atoms, respectively. (e) The charge density difference for studied species, where yellow and cyan colors are charge density concentration and depletion whose value is 0.0002 e/Bohr^3.

Molecular dynamics (MD) simulations

The partial charge of ANF and m-BN molecule was calculated using Gaussian 16 code and the 6-311g(d,p) basis functions were applied. The GAFF force field and Auxiliary Tools of Force Field (AuToFF) were used to parametrize all atoms, such as bond parameters, angle parameters and the dihedral angles, and so on. The number of hydrogen bonds between ANF and m-BN was studied by molecular dynamics (MD)

simulation. In m-BN@ANF ink system, 10 ANF, 20 m-BN and 14675 water molecules were randomly inserted into a cube box with a side length of 8.0 nm; In m-BN dispersion system, 20 m-BN and 14675 water molecules were randomly inserted into a cube box with a side length of 8.0 nm, too. The MD simulations were performed in the GROMACS 2021 software package. The steepest descent method was applied to minimize the initial energy for each system with a force tolerance of 1 kJ (mol^{-1} nm^{-1}) and a maximum step size of 0.002 ps before MD calculations. In all the three directions, periodic boundary conditions were imposed. Leapfrog algorithm was used to integrate the Newtonian equation of motion. The MD simulation was processed in an NPT ensemble and the simulation time is 20 ns. In NPT simulations, the pressure was maintained at 1 bar by the Berendsen barostat in an isotropic manner. The temperature was maintained by the V-rescale thermostat at 298.15 K. The LINCS algorithm was performed for constrain bond lengths of hydrogen atoms. A cutoff of 1.5 nm was employed to calculate the short-range van der Waals interactions and the electrostatic interactions.

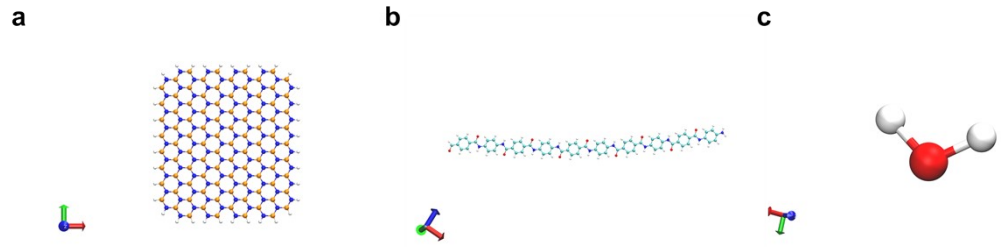

Fig. S7 The molecular dynamics simulation model of (a) m-BN, (b) ANF, and (c) water molecules.

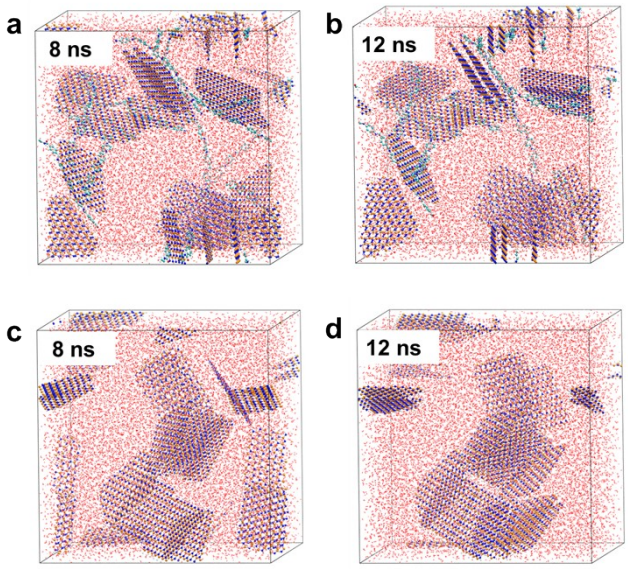

Fig. S8 (a) and (b) snapshots of assembly of m-BN with ANF in water simulated using the GROMACS package. (c) and (d) snapshots of m-BN in water simulated using the GROMACS package.

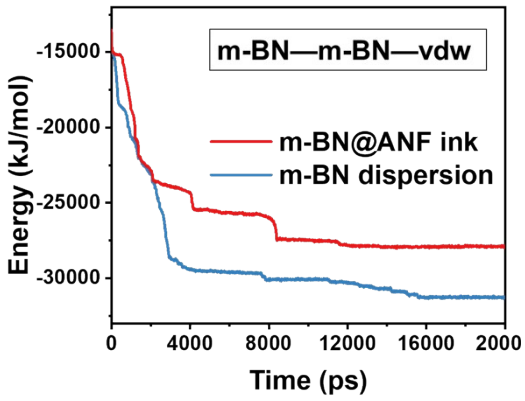

Fig. S9 Van der Waals forces between m-BN in the different systems.

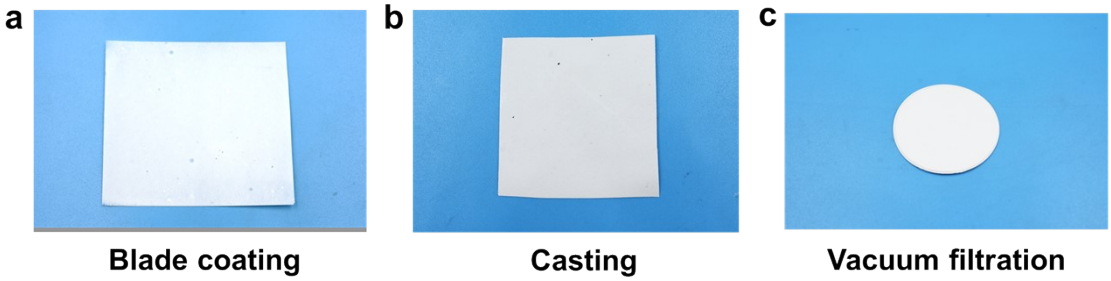

Fig. S10 m-BN@ANF papers formation by (a) blade coating, (b) casting, and (c) vacuum filtration method.

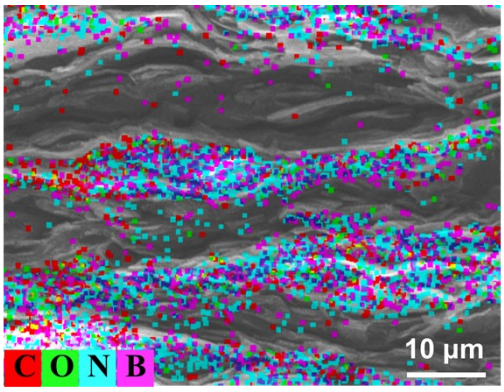

Fig. S11 EDS mapping of m-BN@ANF papers.

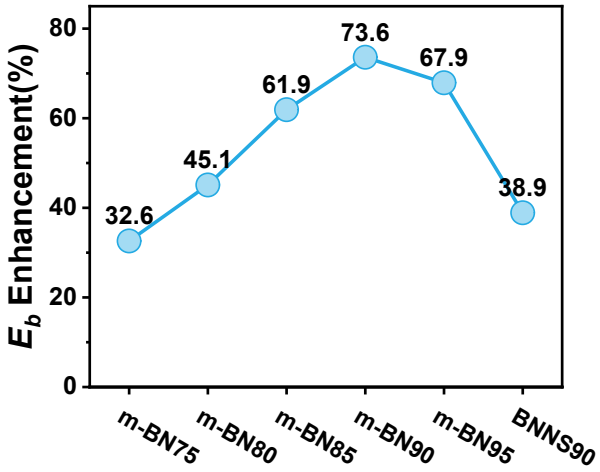

Fig. S12 E_b enhancement of composite papers compared to ANF paper.

Breakdown fracture simulation using phase-field

The physical field used in the model is the electrostatic field. The boundary conditions of the left and right sides of the model are zero charge, a certain voltage is added to the top, and the bottom boundary conditions are set to ground. The dielectric constant of ANF and m-BN are set to 1.5 and 3.9, respectively. The numerical model is converted to screening sites around the breakdown site of the potential matrix to obtain the formation of the breakdown site, and the probability formula for judging whether the breakdown occurs is:

$$p(i',j' \rightarrow i'',j'') = A + B + C \tag{1}$$

$$A = \frac{(\varphi_{i',j'} - \varphi_{i,j} - \varphi_{th})^{\gamma}}{\sum(\varphi_{i',j'} - \varphi_{i,j} - \varphi_{th})^{\gamma}} \tag{2}$$

$$B = (\varphi_{i',j'} - \varphi_{i'',j''} - \varphi_{th})^{\gamma} \tag{3}$$

$$C = -loss \tag{4}$$

where p is the probability of electric branch development. φ_{th} is the threshold potential for electric breakdown of the film. $\varphi_{i,j}$ is the breakdown point potential at which the electric branch has discharged. $\varphi_{i',j'}$ is the next point potential at which discharge may occur. $\varphi_{i'',j''}$ is the electric branch point potential connected with the new discharge point. γ is the fractal dimension, characterizing the irregularity of electric branch development. $loss$ is the loss term of each segment of electric branch development, which represents the difficulty of electric branch development.

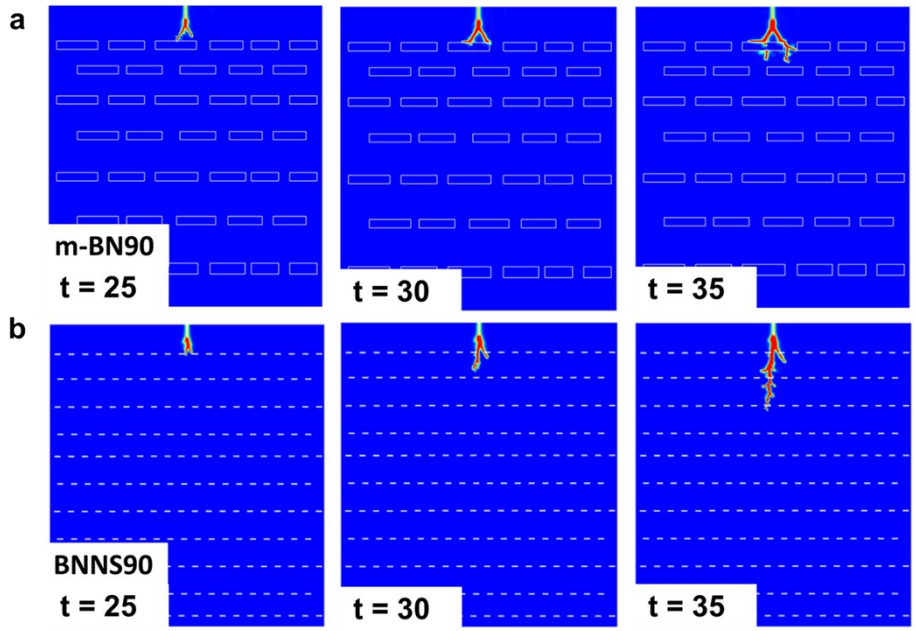

Fig. S13 Finite element simulation of the (a) m-BN90 and (b) BNNS90 models at different times.

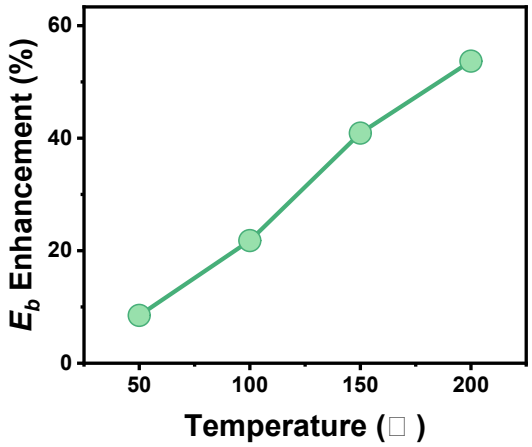

Fig. S14 E_b enhancement of m-BN90 paper at high temperatures compared to 25℃.

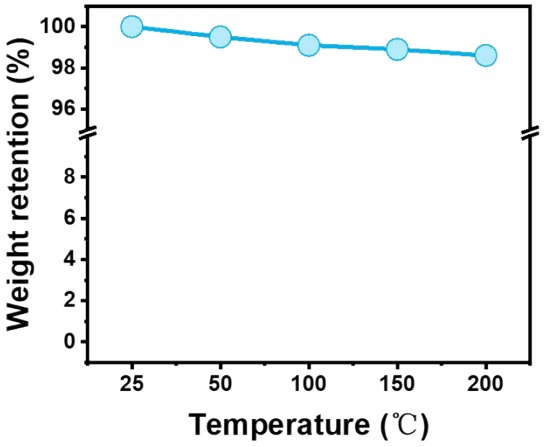

Fig. S15 Mass retention of m-BN90 paper at different temperatures.

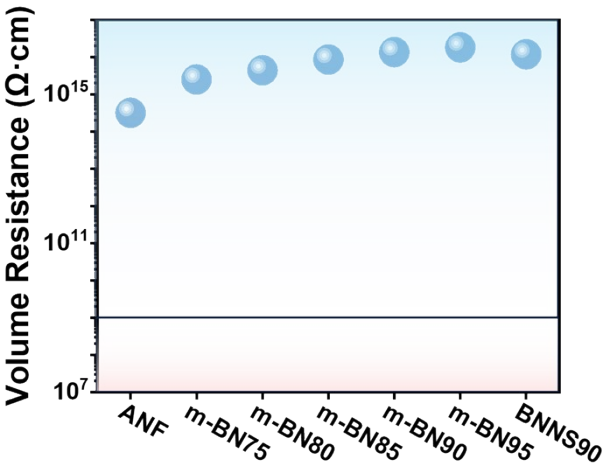

Fig. S16 Volume resistance of m-BN@ANF papers.

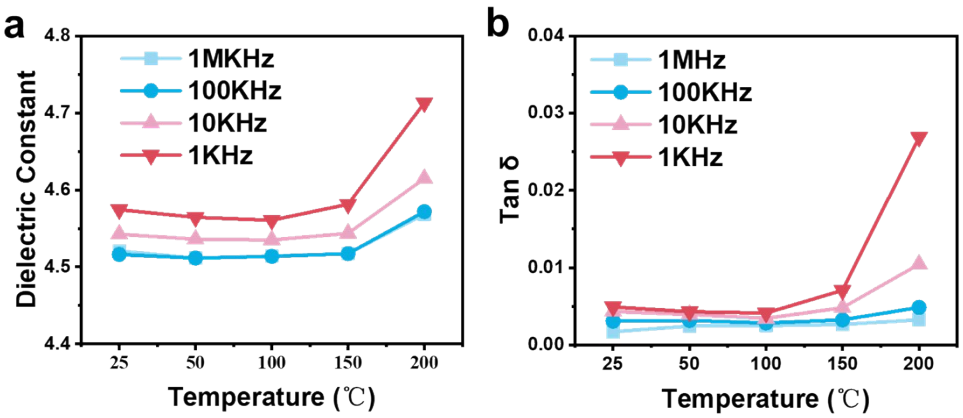

Fig. S17 Dielectric constant and dielectric loss of m-BN90 paper at different temperatures and frequencies.

Table S2. Comparison of the E_b of the m-BN@ANF papers with the previously reported insulating papers at different temperatures.

Materials	Breakdown strength (kV/mm)	Temperature (℃)	Reference
m-BN@ANF	359.0	200	This work
m-BN@ANF	328.9	150	This work
m-BN@ANF	284.5	100	This work
m-BN@ANF	253.5	50	This work
m-BN@ANF	233.5	25	This work
P-APM	184	200	[7]
ANF-RN	176	200	[8]
PI	91	150	[9]
PET1/PVH4	185	125	[10]
BOPP	252.1	120	[11]
PI	105.5	100	[9]

Nomex818	28	25	[12]
BNNSs/PDMS	39.8	25	[13]
ANF-BNNS	59.6	25	[14]
ANF/BNNS	100.7	25	[15]
BC/S-Mica	145.7	25	[16]
ANF-RN	173	25	[8]
P-APM	176	25	[7]

P-APM, RN, PI, PET, PVH4, BOPP, PDMS, and BC indicate pressure-treated aramid nanofiber-polyetherimide-mica, rectorite nanosheets, polyimide, polyethylene terephthalate, polyvinylidene fluoride-hexafluoropropylene, biaxially oriented polypropylene, polydimethylsiloxane and bacterial cellulose, respectively.

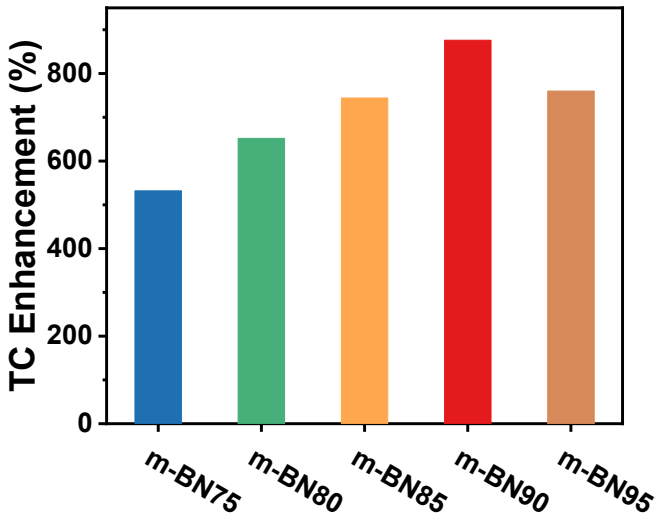

Fig. S18 TC enhancement of m-BN@ANF papers compared to ANF paper.

Heat transfer simulation

Heat transfer performances of composite papers were analyzed with COMSOL Multiphysics 6.0. In a typical simulation, a linear heat source (100 °C) is set at the bottom of the model with a fixed ambient temperature of 25 °C. The area of m-BN model is 5 times that of BNNS model. The thermal conductivity of BN and ANF matrix is set to 400 W/(m·K) and 2.5 W/(m·K), respectively.

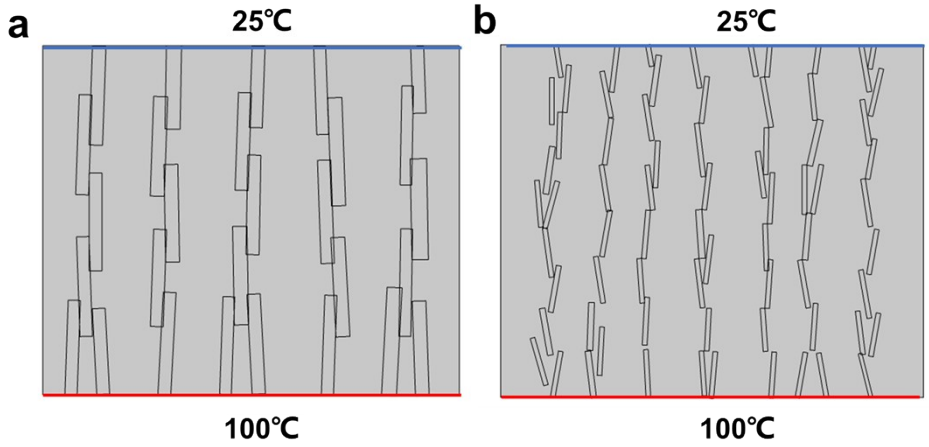

Fig. S19 The models of the (a) m-BN90 paper and (b) BNNS90 paper used in the finite element analysis.

Table S3. The comparison of TC and the specific TC of the m-BN@ANF papers with the other reported BN-base papers prepared by various methods.

Materials	BN content (wt%)	Thermal conductivity (W/(m·K))	Specific thermal conductivity (W/(m·K wt%))	Reference
m-BN@ANF	90	26.4	0.265	This work
PLA/BNNS	20	4.9	0.222	[17]
BNNS/PVA	50	9.3	0.182	[18]
PVDF/BNNS	33.3	10.4	0.291	[19]
BNNS/ANF	45	1.25	0.027	[20]
PANF-BNNS	_	2.4	_	[21]
BNNS@PDA/ANF	50	3.94	0.052	[22]
BNNS/PVA	40	5.25	0.068	[23]
BNNS/EVA	50	13.2	0.254	[24]

CNF/BNNS/MXene	_	19.97	_	[25]
m-BN/PNF	50	9.68	0.197	[26]
APTES-BNNS	50	10.41	0.189	[27]
FeCo/BN/TPU	50	0.6	0.001	[28]
PVA/h-BN	10	6.4	0.620	[29]
BNNSs/PVDF	50	9.26	0.233	[30]

PLA, PVA, PVDF, PDA, EVA, CNF, PNF, APTES, and TPU indicate polylactic acid, poly (vinyl alcohol), polyvinylidene fluoride, polydopamine, ethylene vinyl acetate copolymer, cellulose nanofibers, poly (p-phenylenebenzodioxazole) nanofiber, 3-aminopropyltriethoxysilane, and thermoplastic polyurethane, respectively.

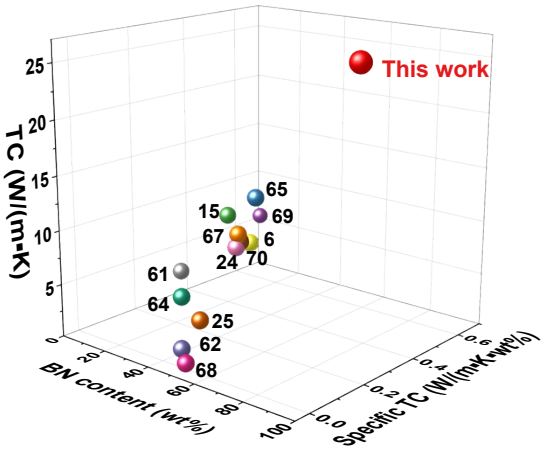

Fig. S20 Comparisons of TC enhancement efficiency of BN and TC to demonstrate the distinct advantage of m-BN@ANF papers.

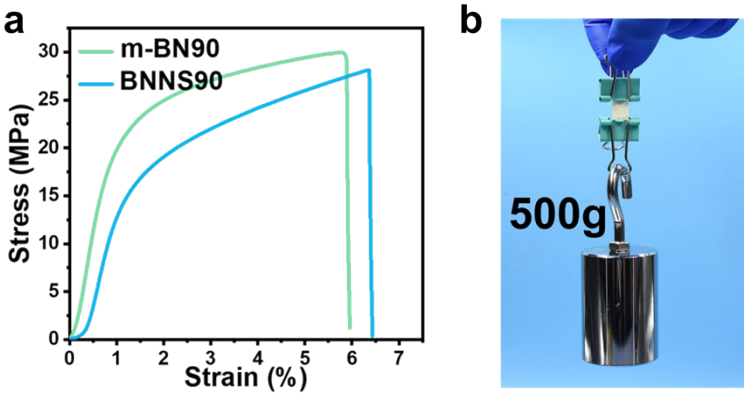

Fig. S21 (a) Stress-strain curve of m-BN90 paper and BNNS90 paper. (b) A small size m-BN90 paper was used to lift a 500 g weight.

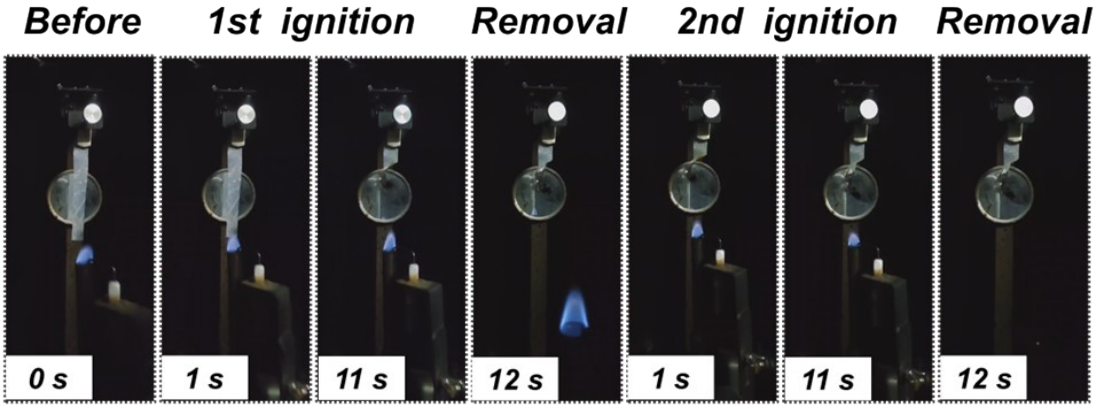

Fig. S22 Snapshots of vertical burning tests for ANF paper.

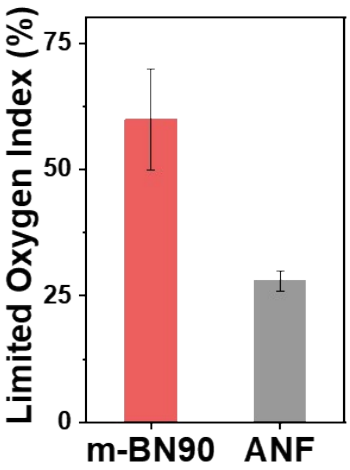

Fig. S23 Limiting oxygen index of m-BN90 and ANF papers.

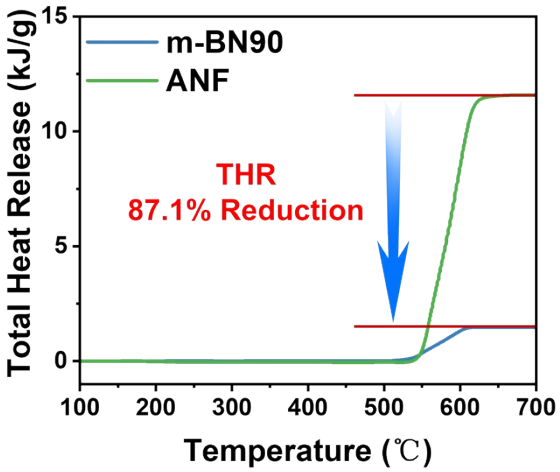

Fig. S24 THR versus temperature curves of m-BN90 and ANF papers.

Table S4. Characteristic parameters of MCC for m-BN@ANF and ANF papers.

Sample	HR Capacity (J/g·K)	PHRR (W/g)	THR (kJ/g)	T_{PHRR} (°C)
m-BN90	27.0	27.3	1.5	582.4
ANF	242.0	244.5	11.6	592.9

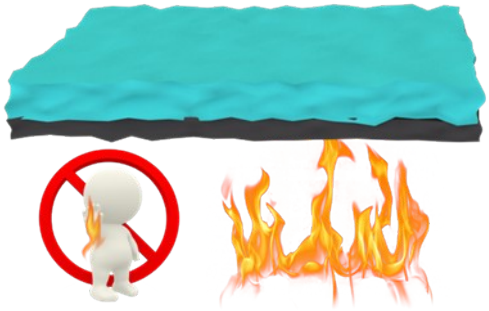

Fig. S25 Flame retardant diagram of m-BN@ANF paper.

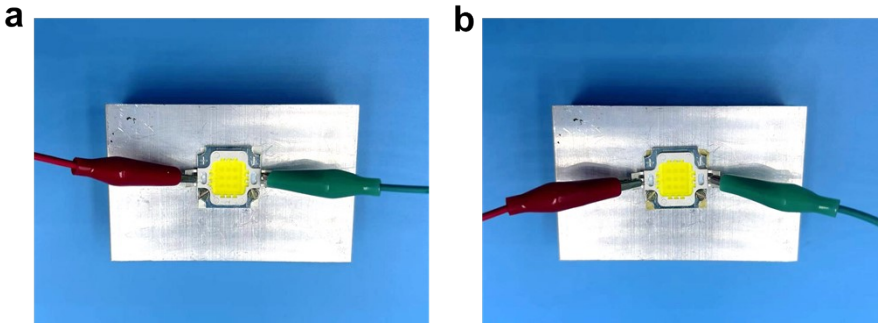

Fig. S26 Digital photographs of (a) m-BN@ANF paper and (b) ANF paper for LED heat transfer.

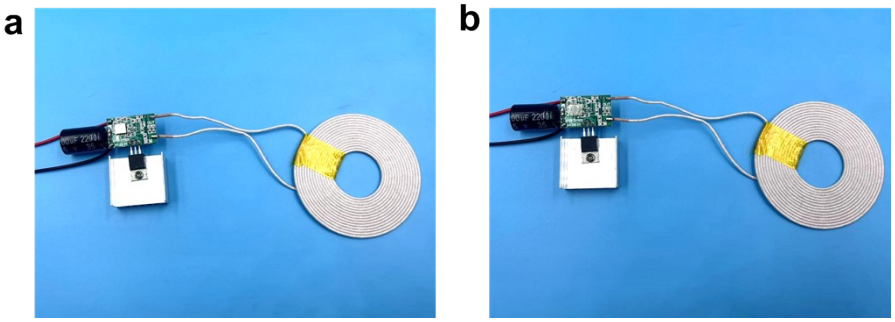

Fig. S27 Digital photographs of (a) m-BN@ANF paper and (b) ANF paper for wireless charging device heat transfer.

References

1 G. Kresse and J. Furthmüller, *Phys. Rev. B*, 1996, **54**, 11169–11186.

2 G. Kresse and D. Joubert, *Phys. Rev. B*, 1999, **59**, 1758–1775.

3 J. P. Perdew, J. A. Chevary, S. H. Vosko, K. A. Jackson, M. R. Pederson, D. J. Singh and C. Fiolhais, *Phys. Rev. B*, 1992, **46**, 6671–6687.

4 S. Grimme, J. Antony, S. Ehrlich and H. Krieg, *J. Chem. Phys.*, 2010, **132**, 154104.

5 L. Ma, J.-M. Zhang, K.-W. Xu and V. Ji, *Appl. Surf. Sci.*, 2015, **343**, 121–127.

6 Z. Gao, W. Yang, X. Ding, G. Lv and W. Yan, *Appl. Surf. Sci.*, 2018, **436**, 585–595.

7 X. Pan, Z. Bao, W. Xu, H. Gao, B. Wu, Y. Zhu, G. Yu, J. Chen, S. Zhang, L. Li, H. Wu, X. Li and S. Yu, *Adv. Funct. Mater.*, 2023, **33**, 2210901.

8 X. Pan, G. Yu, H. Gao, Z. Wang, Z. Bao, X. Li and S. Yu, *Adv. Mater.*, 2022, **34**, 2206855.

9 Y. Min, J. Yu, P. Xu, P. Li, S. Luo, B. Chu and S. Yu, *ACS Appl. Mater. Interfaces*, 2022, **14**, 51265–51274.

10 Q. Feng, Y. Zhang, D. Liu, Y. Song, L. Huang and Z. Dang, *Mater. Today Energy*, 2022, **29**, 101132.

11 J. Wang, H. Guo, S. Zeng, J. Du, Q. Zhang and K. Wang, *Chem. Eng. J.*, 2024, **492**, 152237.

12 F. Zeng, X. Chen, G. Xiao, H. Li, S. Xia and J. Wang, *ACS Nano*, 2020, **14**, 611–619.

13 M. Li, M. Wang, X. Hou, Z. Zhan, H. Wang, H. Fu, C. Lin, L. Fu, N. Jiang and J. Yu, *Compos. B: Eng*, 2020, **184**, 107746.

14 M. Li, Y. Zhu and C. Teng, *Compos. Commun.*, 2020, **21**, 100370.

15 N. Li, Z. Lu, X. Ji, D. Ning, N. Yan and S. E, *ACS Appl. Nano Mater.*, 2024, **7**, 9925–9933.

16 W. Sun, Z. Han, X. Yue, H. Zhang, K. Yang, Z. Liu, D. Li, Y. Zhao, Z. Ling, H. Yang, Q. Guan and S. Yu, *Adv. Mater.*, 2023, **35**, 2300241.

17 R. Wu, X. Song, Y. Ji, H. Wu, S. Guo and J. Qiu, *Compos. Sci. Technol.*, 2024, **251**, 110573.

18 T. Wang, G. Zhang, B. Zhang, S. Liu, D. Li and C. Liu, *ACS Appl. Nano Mater.*, 2021, **4**, 4153–4161.

19 J. Chen, X. Huang, B. Sun and P. Jiang, *ACS Nano*, 2019, **13**, 337–345.

20 R. Tian, X. Jia, M. Lan, J. Yang, S. Wang, Y. Li, D. Shao, L. Feng and H. Song, *Chem. Eng. J.*, 2022, **446**, 137255.

21 M. M. Rahman, A. B. Puthirath, A. Adumbumkulath, T. Tsafack, H. Robatjazi, M. Barnes, Z. Wang, S. Kommandur, S. Susarla, S. M. Sajadi, D. Salpekar, F. Yuan, G. Babu, K. Nomoto, S. Islam, R. Verduzco, S. K. Yee, H. G. Xing and P. M. Ajayan, *Adv. Funct. Mater.*, 2019, **29**, 1900056.

22 T. Ma, Y. Zhao, K. Ruan, X. Liu, J. Zhang, Y. Guo, X. Yang, J. Kong and J. Gu, *ACS Appl. Mater. Interfaces*, 2020, **12**, 1677–1686.

23 S. Chen, R. Xu, J. Liu, X. Zou, L. Qiu, F. Kang, B. Liu and H. Cheng, *Adv. Mater.*, 2019, **31**, 1804810.

24 Z. Wang, W. Liu, Y. Liu, Y. Ren, Y. Li, L. Zhou, J. Xu, J. Lei and Z. Li, *Compos. B. Eng.*, 2020, **180**, 107569.

25 Y. Shang, Y. Ji, J. Dong, G. Yang, X. Zhang, F. Su, Y. Feng and C. Liu, *Compos. Sci. Technol.*, 2021, **214**, 108974.

26 L. Tang, K. Ruan, X. Liu, Y. Tang, Y. Zhang and J. Gu, *Nano-Micro Lett.*, 2023, **16**, 38.

27 H. Tu, K. Xie, X. Lin, R. Zhang, F. Chen, Q. Fu, B. Duan and L. Zhang, *J. Mater. Chem. A*, 2021, **9**, 10304–10315.

28 M. Se Chang, S. Hwang, S. Jeong, J. Won Jeong, B. Park, S. Yang, C. Rae Park and Y. Kwon, *Chem. Eng. J.*, 2023, **475**, 146496.

29 O. H. Kwon, T. Ha, D.- Kim, B. G. Kim, Y. S. Kim, T. J. Shin, W. Koh, H. S. Lim and Y. Yoo, *ACS Appl. Mater. Interfaces*, 2018, **10**, 34625–34633.

30 C. Teng, L. Su, J. Chen and J. Wang, *Compos. Part A Appl. Sci. Manuf.*, 2019, **124**, 105498.